NANO LETTERS

Letter

pubs.acs.org/NanoLett

Electron Mobilities Approaching Bulk Limits in "Surface-Free" GaAs Nanowires

Hannah J. Joyce,*[,†] Patrick Parkinson,[‡] Nian Jiang,[§] Callum J. Docherty,[‡] Qiang Gao,[§] H. Hoe Tan,[§] Chennupati Jagadish,[§] Laura M. Herz,[‡] and Michael B. Johnston*[,‡]

[†]Department of Engineering, University of Cambridge, 9 JJ Thomson Avenue, Cambridge, Cambridgeshire CB3 0FA, United Kingdom

[‡]Department of Physics, University of Oxford, Clarendon Laboratory, Parks Road, Oxford, Oxfordshire, OX1 3PU, United Kingdom

[§]Department of Electronic Materials Engineering, Research School of Physics and Engineering, Australian National University, Canberra, ACT 0200, Australia

Supporting Information

ABSTRACT: Achieving bulk-like charge carrier mobilities in semiconductor nanowires is a major challenge facing the development of nanowire-based electronic devices. Here we demonstrate that engineering the GaAs nanowire surface by overcoating with optimized AlGaAs shells is an effective means of obtaining exceptionally high carrier mobilities and lifetimes. We performed measurements of GaAs/AlGaAs core−shell nanowires using optical pump-terahertz probe spectroscopy: a noncontact and accurate probe of carrier transport on ultrafast time scales. The carrier lifetimes and mobilities both improved significantly with increasing AlGaAs shell thickness. Remarkably, optimized GaAs/AlGaAs core−shell nanowires exhibited electron mobilities up to 3000 $cm^2 V^{-1} s^{-1}$, reaching over 65% of the electron mobility typical of high quality undoped bulk GaAs at equivalent photoexcited carrier densities. This points to the high interface quality and the very low levels of ionized impurities and lattice defects in these nanowires. The improvements in mobility were concomitant with drastic improvements in photoconductivity lifetime, reaching 1.6 ns. Comparison of photoconductivity and photoluminescence dynamics indicates that midgap GaAs surface states, and consequently surface band-bending and depletion, are effectively eliminated in these high quality heterostructures.

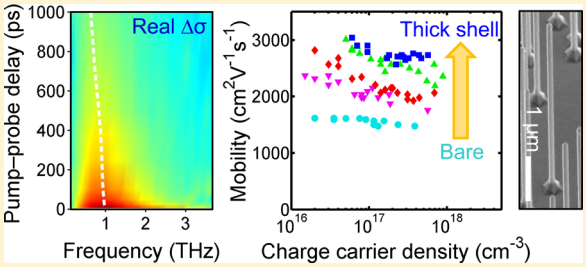

KEYWORDS: *GaAs, nanowire, terahertz, photoconductivity, lifetime, mobility*

GaAs nanowires and associated heterostructures are currently inspiring a host of new device concepts,[1−3] ranging from nanowire-based photovoltaics[4−6] to single photon emitters.[7] Recently, room temperature operation of GaAs/AlGaAs core−shell nanowire lasers was demonstrated,[8,9] and studies of single-nanowire devices revealed the potential of GaAs nanowire-based solar cells to achieve efficiencies exceeding the Shockley−Queisser limit.[4]

Despite their clear potential, two obstacles have arisen in the development of GaAs nanowire-based devices. First, the GaAs material system suffers from the influence of midgap surface states: a problem which is compounded for GaAs nanowires owing to their large surface area-to-volume ratios. Consequently, bare GaAs nanowires exhibit surface-mediated depletion of charge carriers,[10−15] an extremely high surface recombination velocity of 10^5 to 10^6 cm/s,[12,16] and extremely short carrier lifetimes of only a few picoseconds.[16,17] The favored solution is overcoating GaAs cores with AlGaAs shells which passivate the underlying GaAs surface.[18−21] These "surface-free" nanowires can achieve carrier lifetimes beyond 1 ns at cryogenic temperatures and at room temperature.[22,23]

The second problem has received far less attention to date: GaAs nanowires typically exhibit significantly lower carrier mobilities than their bulk counterparts. Reported electron and hole mobilities for bare GaAs nanowires are commonly lower than 1500 $cm^2 V^{-1} s^{-1}$ and 100 $cm^2 V^{-1} s^{-1}$, respectively.[13,16,24] Although the elimination of planar crystallographic defects achieved appreciable improvements in electron mobility,[17] bulk-like mobilities have remained elusive. Furthermore, it is unclear whether it is ionized impurity scattering[13] or surface-mediated scattering[16] that limits the carrier mobility more severely. As most device applications demand high carrier mobilities and long diffusion lengths, understanding the limitations on carrier mobility and improving the mobility are of paramount importance for nanowire-based electronics.

Progress toward high mobility GaAs nanowires has been further hindered by challenges in making accurate measurements of mobility. Among these challenges are the difficulties in obtaining ohmic contacts to GaAs nanowires,[13] the uncertainty

Received: August 7, 2014
Revised: September 2, 2014
Published: September 18, 2014

introduced by the gate capacitance term in field-effect mobility measurements,[25] and the nanowires' quasi one-dimensional geometry which precludes conventional Hall effect measurements unless specialized procedures are employed for making electrical contacts to the nanowires.[26]

In this Letter, we investigate engineering the GaAs nanowire surface as a means of achieving bulk-like mobilities. Remarkably, overcoating the GaAs cores with optimized AlGaAs shells improved the electron mobility to at least 65% of the mobility of high quality bulk GaAs at similar carrier densities. The optimized AlGaAs shells also drastically improved the photoconductivity lifetime, which reached 1.6 ns for the highest quality sample. We employ optical pump−terahertz probe (OPTP) spectroscopy to measure carrier transport and dynamics at room temperature. As a noncontact technique, OPTP spectroscopy circumvents the aforementioned problems associated with traditional contact-based electrical measurements. It is therefore ideally suited to studies of GaAs nanowires.[27] We also perform time-resolved photoluminescence (PL) measurements, which provide complementary information on the localization and temporal evolution of electron and hole populations after photoexcitation.

Nanowires were grown on GaAs (111)B substrates by metal−organic chemical vapor deposition (MOCVD) using trimethylgallium (TMGa), trimethylaluminum (TMAl) and arsine precursors. Au nanoparticles were employed to direct nanowire growth via the vapor−liquid−solid mechanism. A low temperature (375 °C) growth procedure was used to grow GaAs cores with twin-free zinc-blende crystal structure, minimal tapering, and uniform diameters of 50 ± 5 nm.[28] Figure 1a shows a scanning electron microscope (SEM) image of a typical bare GaAs nanowire. For AlGaAs shell growth, the vapor phase fraction TMAl/(TMAl + TMGa) was $\chi_{v,Al} = 0.5$, yielding a shell composition of $Al_{0.4}Ga_{0.6}As$.[29] Shells were then grown around the cores at a high temperature (750 °C) conducive to conformal shell growth. Several samples were grown, each with a particular AlGaAs shell thickness tailored by varying the shell growth time. Shell thicknesses between 5 and 34 nm were achieved with shell growth times between 60 and 480 s. Figure 1b−d shows SEM images of these GaAs/AlGaAs core−shell nanowires. Finally, a thin GaAs cap layer was grown for 5 min at 750 °C, to protect the underlying AlGaAs shell from oxidation. The resulting core−shell−cap nanowires are illustrated in Figure 1e−h. Core−shell−cap nanowires were stored in air, whereas core−shell nanowires were stored in N_2 to prevent oxidation of the AlGaAs shell. Shell thicknesses were measured using cross-sectional transmission electron microscope (TEM) images as illustrated in the Supporting Information (Figure S1). The nanowires were transferred to z-cut quartz substrates for terahertz and PL measurements. The quartz substrates are most suitable for these experiments, because they, unlike the GaAs growth substrate, do not exhibit any photoconductivity or photoluminescence response that could otherwise obscure the nanowire response.

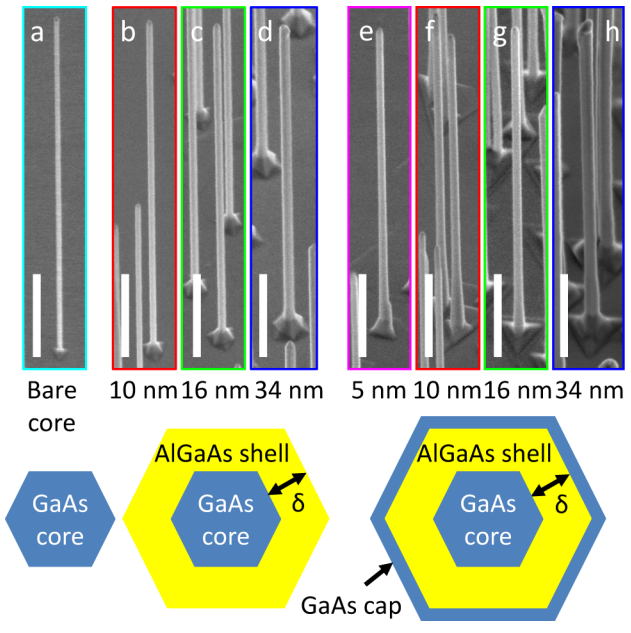

Figure 1. SEM images of nanowires as-grown on GaAs substrates: (a) a bare GaAs nanowire, (b−d) GaAs/AlGaAs core−shell nanowires, and (e−h) GaAs/AlGaAs/GaAs core−shell−cap nanowires. The AlGaAs shell thicknesses are (e) 5 nm (b and f) 10 nm, (c and g) 16 nm, and (d and h) 34 nm. Scale bars are 1 μm. Images were taken at a tilt of 40°. Schematic diagrams of the nanowire cross sections are shown beneath the SEM images, where δ represents the AlGaAs shell thickness.

OPTP measurements were performed using a terahertz spectroscopy system that is described in detail in our previous work.[30] The nanowires were photoexcited using pump pulses centered at 800 nm, of 35 fs duration, and with fluence between 1 and 200 $\mu J/cm^2$/pulse. This photoexcitation induces a change, $\Delta E(t)$, in the transmission of a weak terahertz probe pulse of electric field $E(t)$. The relative change, $\Delta E/E$, is proportional to the conductivity of the nanowires. Measured values of $\Delta E/E$ were converted to nanowire photoconductivity, $\Delta\sigma$, taking into account the areal density and diameters of the nanowires on quartz.[30] The measured photoconductivity arises predominantly from photoexcited electrons, because the effective mass of holes in GaAs is significantly larger than that of electrons. In addition, time-resolved PL measurements were performed on the same samples using time-correlated single photon counting (TCSPC) and PL up-conversion, as described in the Supporting Information. For PL measurements, the nanowire ensembles were photoexcited with pulses of fluence 3 $\mu J/cm^2$/pulse, centered at 770 nm for TCSPC and at 750 nm for up-conversion. Photoluminescence was detected at the peak of the PL spectrum (Supporting Information Figure S2), at 865 nm (1.43 eV), which corresponds to the band-edge of the GaAs core. All measurements were performed at room temperature. Each of the photoexcitation energies used for OPTP spectroscopy, TCSPC, and PL up-conversion lies below the bandgap of the $Al_{0.4}Ga_{0.6}As$ shells and, therefore, selectively photoexcites the GaAs only.

Our first observation is the pronounced effect of AlGaAs shell thickness on the photoconductivity lifetime. Figure 2a plots photoconductivity decays of core−shell−cap nanowires with different AlGaAs shell thicknesses. Monoexponential functions provided good fits to the transients at times greater than 100 ps after photoexcitation. The photoconductivity lifetime increased with increasing AlGaAs shell thickness, reaching 1.3 ns for the thickest shells. This phenomenon is readily explained by considering tunneling through the AlGaAs shell, as modeled for similar nanowires by Jiang et al.[29] Briefly, there is a finite probability that carriers in the nanowire core tunnel through the AlGaAs barrier and recombine at the outer GaAs cap surface, where the surface recombination velocity is

dx.doi.org/10.1021/nl503043p | Nano Lett. 2014, 14, 5989−5994

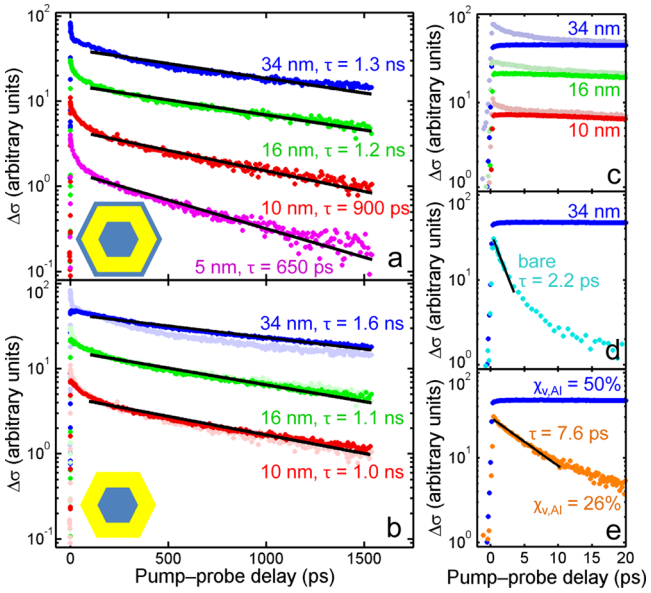

Figure 2. Transient photoconductivity ($\Delta\sigma$) decays. (a) $\Delta\sigma$ decays for GaAs/AlGaAs/GaAs core–shell–cap nanowires with AlGaAs shell thicknesses of 5, 10, 16, and 34 nm, as labeled for each curve. (b and c) $\Delta\sigma$ decays for GaAs/AlGaAs core–shell nanowires with AlGaAs shell thicknesses of 10, 16, and 34 nm, as labeled for each curve. To allow comparison between core–shell and core–shell–cap nanowires with equal shell thicknesses, data from (a) are shown in the background with faint symbols. The first 20 ps after photoexcitation is magnified in (c). (d) $\Delta\sigma$ decays for bare GaAs nanowires and for optimally passivated GaAs/AlGaAs core–shell nanowires with 34 nm thick AlGaAs shells. (e) $\Delta\sigma$ decays for GaAs/AlGaAs core–shell nanowires with 30 nm thick AlGaAs shells grown with $\chi_{v,Al}$ = 0.26 at 650 °C, and for optimally passivated GaAs/AlGaAs core–shell nanowires grown with $\chi_{v,Al}$ = 0.5 at 750 °C. The photoexcitation pump fluence was 10 μJ/cm^2. Decays are scaled for clarity. Straight lines are mono-exponential fits to the decays, with time constants labeled.

10^5 to 10^6 cm/s.[16] The probability of tunneling decreases exponentially with increasing barrier thickness, and consequently the photoconductivity lifetime in the core increases.

Figure 2b plots photoconductivity decays for core–shell nanowires, which lack the outer GaAs cap. As with the core–shell–cap nanowires, the lifetime increases with increasing shell thickness. This indicates that even in the absence of an outer GaAs cap, deep surface states exist at the outer AlGaAs surface, to which carriers can tunnel and at which these carriers recombine. For equivalent AlGaAs shell thicknesses, the core–shell and the core–shell–cap nanowires show comparable lifetimes. This is expected, because the surface recombination velocity of bare AlGaAs surfaces is generally reported to be similar to that of bare GaAs surfaces.[31] The core–shell nanowires with the thickest (34 nm) AlGaAs shells exhibited the longest photoconductivity lifetime, of 1.6 ns.

We refrain from detailed analysis of the first 100 ps after photoexcitation, as this is strongly influenced by the GaAs cap layer, rather than by the quality of the AlGaAs shell. Specifically, the core–shell–cap nanowires exhibit a sharp decay within the first 100 ps of photoexcitation. In Figure 2b,c, it is clear that this rapid component is pronounced for the core–shell–cap nanowires but is not observed for the core–shell nanowires. This leads us to attribute the rapid early decay to the carrier population initially photogenerated in the GaAs cap, which recombines rapidly at the GaAs cap surface. To add further support to this explanation, we note that for each core–shell–cap sample, the amplitude of the rapidly decaying component is between 15% and 35% of the total photoconductivity signal. These proportions are comparable to the ratio of the GaAs cap volume to the total GaAs volume of the nanowires.

Finally, Figure 2d,e emphasizes the passivating role of the high quality AlGaAs shells. The photoconductivity of bare GaAs nanowires (Figure 2d) decays to less than half its maximum value within 2 ps. The decay is not single exponential: it is initially rapid and then slows as surface traps become filled.[17] In marked contrast, the photoconductivity of the optimally passivated core–shell nanowires, with 34 nm thick AlGaAs shells and 1.6 ns lifetimes, shows negligible decay over the first 20 ps after photoexcitation.

Figure 2e compares the optimally passivated core–shell nanowires with nanowires grown using an earlier, unoptimized procedure for AlGaAs shell growth.[17] For the unoptimized nanowires, the GaAs cores were grown under identical conditions to the optimally passivated core–shell nanowires, but the 30 nm thick AlGaAs shells were grown with a vapor phase Al fraction of $\chi_{v,Al}$ = 0.26 and at a temperature of 650 °C. These unoptimized core–shell nanowires exhibit a rapid photoconductivity decay (Figure 2e), where the lifetime immediately after photoexcitation is less than 8 ps. In contrast, the photoconductivity lifetime of the optimally passivated core–shell nanowires, at 1.6 ns, is over 2 orders of magnitude longer. This difference is despite the comparable thicknesses of the optimized and unoptimized shells. Two effects are responsible for improving the lifetime of the optimized core–shell nanowires, namely, (i) the higher AlGaAs growth temperature lowers the interfacial recombination velocity at the GaAs/AlGaAs interface,[23,32] and (ii) the higher Al content raises the potential barrier for carriers tunneling between the core and the outer nanowire surface. Clearly, the quality, composition and thickness of the AlGaAs shells are important parameters for effective passivation.

To gain further insight into charge carrier dynamics, we performed time-resolved PL measurements via TCSPC and PL up-conversion. Figure 3 compares PL and photoconductivity

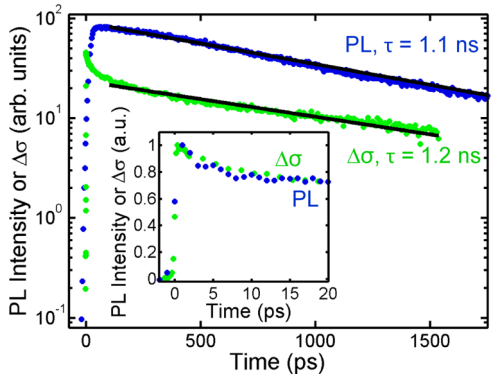

Figure 3. Comparison of photoconductivity ($\Delta\sigma$) and photoluminescence decays for core–shell–cap nanowires with 16 nm thick AlGaAs shells. The photoexcitation pump fluence was 10 μJ/cm^2 for OPTP measurements and 3 μJ/cm^2 for time-resolved PL measurements. The main figure shows time-resolved PL measured by TCSPC, which has a system temporal resolution of 40 ps. The inset shows time-resolved PL measured by PL up-conversion, which has a higher temporal resolution of 0.25 ps. All measurements were performed at room temperature.

dx.doi.org/10.1021/nl503043p | Nano Lett. 2014, 14, 5989–5994

decays on long (hundreds of picoseconds) and short (picosecond) time scales for core−shell−cap nanowires with 16 nm thick AlGaAs shells. The decay dynamics measured at early times by PL up-conversion (inset of Figure 3) are comparable to the photoconductivity dynamics. At later times the PL and photoconductivity decays remain similar. A single exponential fit to the TCSPC data yields a carrier lifetime of 1.1 ns, which is marginally shorter than the photoconductivity lifetime of 1.2 ns. This small difference can be explained considering the differences between the PL and photoconductivity measurements. PL measures the product of the electron and hole density distributions. Photoconductivity, in contrast, measures the product of the photoexcited electron density and electron mobility, both of which change as a function of time after photoexcitation. Carrier mobility tends to increase as the carrier density drops, due to decreased carrier−carrier scattering, as will be discussed later. Consequently, photoconductivity lifetimes tend to be longer than PL lifetimes, as seen in Figure 3.

The overall similarity between the PL and photoconductivity dynamics is notable. This is in marked contrast to our previous study of InP nanowires, which demonstrated over 2 orders of magnitude in difference between the band-edge PL and photoconductivity decay rates.[30,33] In the case of InP nanowires, this disparity was a signature of the high level of zinc-blende−wurtzite polytypism, which spatially separated electrons and holes to rapidly quench band-edge PL,[30,33] while prolonging the lifetime of lower energy PL.[34] In the current study, the GaAs/AlGaAs core−shell nanowires are purely zinc-blende without twin defects,[28] so this degree of electron−hole separation is not expected, and indeed, not observed.

Furthermore, the similarity between PL and photoconductivity dynamics, indicating that spatial separation of electrons and holes is minimal, in turn suggests that surface band-bending at the core−shell interface is minimal. This contrasts with bare GaAs nanowires, which exhibit surface Fermi level pinning at deep surface states approximately 0.5 eV above the valence band maximum: these states give rise to strong band-bending effects at the nanowire surface to spatially separate electrons and holes.[35,36] This absence of strong band-bending effects in our GaAs/AlGaAs core−shell heterostructures is further evidence that midgap surface states are eliminated by high quality AlGaAs shells.

We next turn to photoconductivity spectra, as a contact-free and accurate means of determining carrier mobility. Each spectrum measures the frequency-dependent conductivity at a fixed delay after photoexcitation at a fixed fluence. Figure 4 shows typical spectra obtained for GaAs/AlGaAs/GaAs core−shell−cap nanowires, at different times after photoexcitation. The spectra show a clear Lorentzian component, with a resonant frequency that blue-shifts with increasing carrier density. This is characteristic of localized surface plasmon (LSP) modes, which have previously been observed in terahertz and mid-infrared studies of III−V, Si and Ge nanowires.[17,37,38] Excellent fits to the spectral data were obtained following the procedure outlined in our previous studies,[17,39] assuming the conductivity, $\Delta\sigma$, includes both a Drude-like free carrier response and a surface plasmon response: $\Delta\sigma = \Delta\sigma_{\mathrm{Drude}} + \Delta\sigma_{\mathrm{Plasmon}}$. The Drude and surface plasmon components are given by

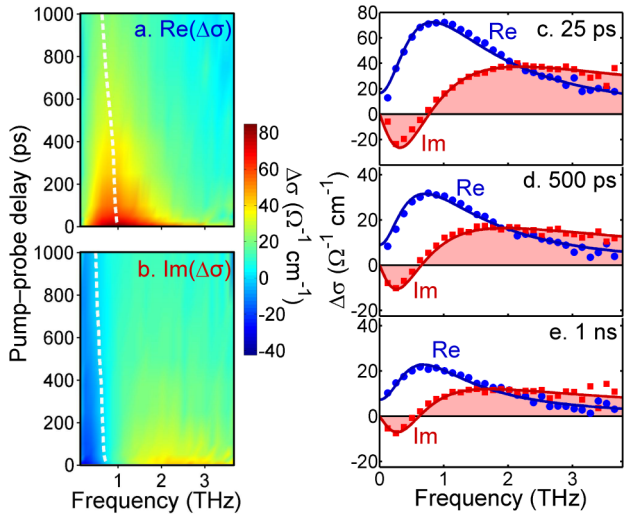

Figure 4. Frequency-dependent photoconductivity at different times after photoexcitation, measured for core−shell−cap nanowires with 16 nm thick AlGaAs shells. The photoexcitation pump fluence was 10 μJ/cm^2. Real and imaginary parts of the photoconductivity are shown in the color maps of (a) and (b), respectively. The white dashed line in (a) plots the maximum of the real part of the photoconductivity. The white dashed line in (b) plots the zero-crossing of the imaginary part of the photoconductivity. Photoconductivity spectra obtained at 25 ps, 500 ps, and 1 ns after photoexcitation are shown in (c), (d), and (e), respectively. The symbols are the measured data, and the lines are the fitted responses. The real (blue circles and lines) and imaginary (red squares and lines) components of the conductivity are plotted.

$$\Delta\sigma_{\mathrm{Drude}} = \frac{iN_{\mathrm{dr}}e^2\omega}{m_e^*(\omega^2 + i\omega\gamma)} \quad (1)$$

$$\Delta\sigma_{\mathrm{Plasmon}} = \frac{iN_{\mathrm{pl}}e^2\omega}{m_e^*(\omega^2 - \omega_{\mathrm{pl}}^2 + i\omega\gamma)} \quad (2)$$

respectively. Here, N_{dr} and N_{pl} are the carrier densities in the Drude and surface plasmon modes, respectively, e is the electronic charge, m_e^* is the electron effective mass, ω_{pl} is the surface plasmon resonance frequency and γ is the momentum scattering rate. To fit the spectra, it was not necessary to include any contribution from unintentional dopants.[16] The momentum scattering rate can be converted to electron mobility via

$$\mu = \frac{e}{m_e^*\gamma} \quad (3)$$

Spectra were measured at different photoexcitation fluences and different times after photoexcitation. Fits to each of these spectra allowed the determination of electron scattering rate and electron mobility at a particular carrier density. Figure 5 plots the carrier density-dependent scattering rates and mobilities determined for our series of bare GaAs nanowires and core−shell−cap nanowires. Each data point in Figure 5 corresponds to a single spectrum. For core−shell−cap nanowires, spectra were obtained at probe delay times at least 25 ps after photoexcitation. By this time, the carrier density in the GaAs cap has decayed to negligible levels, as discussed earlier, so that the measured spectra can confidently be attributed to the GaAs core alone.

For all samples, the frequency of scattering events increased and the electron mobility decreased with increasing carrier

dx.doi.org/10.1021/nl503043p | Nano Lett. 2014, 14, 5989−5994

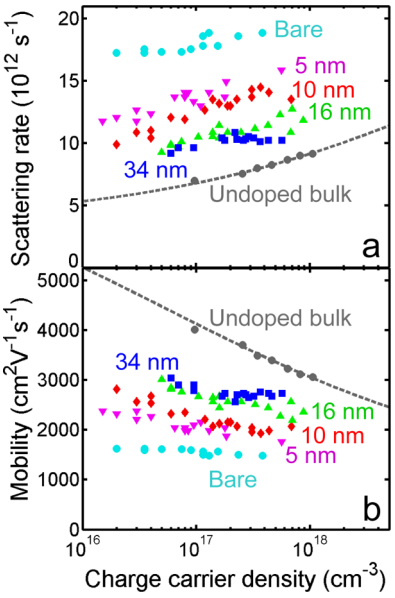

Figure 5. Carrier density-dependent electron scattering rates (a) and electron mobilities (b), measured for bare GaAs nanowires (light blue circles) and GaAs/AlGaAs core–shell–cap nanowires with AlGaAs shell thicknesses of 5 nm (magenta triangles), 10 nm (red diamonds), 16 nm (green triangles), and 34 nm (blue squares). Scattering rates, mobilities and photoexcited carrier densities were extracted from photoconductivity spectra obtained at photoexcitation fluences between 1 and 200 $\mu J/cm^2$/pulse and times between 25 and 1000 ps after photoexcitation. Electron mobilities, determined by Sharma et al.,[41] for photoexcited undoped bulk GaAs are also shown (gray circles). The dashed line is an empirical fit to the bulk data using the Caughey-Thomas relation.[41,42] All measurements of electron mobility were performed at room temperature.

density. This is typical of bulk semiconductors, and occurs due to the higher rate of carrier–carrier scattering at higher carrier densities.[40,41] The bare GaAs nanowires featured the lowest mobilities, in the region of 1500 cm^2 V^{-1} s^{-1}. The core–shell–cap nanowires exhibited considerably higher mobilities, and these mobilities increased with increasing AlGaAs shell thickness. The highest mobilities, up to 3000 cm^2 V^{-1} s^{-1}, were obtained for the samples with 16 and 34 nm thick AlGaAs shells (Figure 5).

For comparison, Figure 5 also plots scattering rates and electron mobilities measured for high quality undoped bulk GaAs, over the same range of photoexcited carrier densities.[41] Throughout the range of measured carrier densities, the core–shell–cap nanowires with 16 and 34 nm thick AlGaAs shells exhibit electron mobility values of over 65% of those observed in bulk GaAs.

The improvement in carrier mobility afforded by the AlGaAs shell overcoating can be explained considering the role of the nanowire surface in carrier scattering. In bare GaAs nanowires, charged surface states, together with surface roughness, will scatter carriers in the vicinity of the GaAs surface.[43] When an AlGaAs shell is present, carriers in the GaAs core are spatially separated from charged surface states, which would otherwise scatter carriers. Thicker shells give greater separation from these scattering sites, thereby increasing the carrier mobility. Similarly, surface passivation has been shown to improve mobilities in Ge/Si core–shell nanowires,[44] and in InAs/InP core–shell nanowires.[25] We observe a large difference in mobilities between bare and AlGaAs coated nanowires, indicating that surface-mediated scattering is the dominant process limiting the carrier mobility in bare GaAs nanowires. Furthermore, the high mobilities observed for AlGaAs coated nanowires suggest that scattering from interface roughness, ionized impurities and other lattice defects is minimal. This points to the very high quality of the GaAs core and the GaAs/AlGaAs interface.

We anticipate that in core–shell–cap nanowires, both the AlGaAs shell and the GaAs cap, contribute to the improvement in mobility, as both shell and cap play a role in spatially separating carriers in the core from the nanowire surface. As expected, for a given AlGaAs shell thickness, core–shell–cap nanowires exhibit higher electron mobilities than core–shell nanowires which lack the GaAs cap (see Supporting Information Figure S3).

We also consider the effect of annealing, as an alternative explanation for the improved carrier mobility with increasing AlGaAs shell thickness. Annealing could conceivably play a role, given that shell and cap growth was performed a high temperature of 750 °C, compared to nanowire core growth (375 °C). Nanowires with thicker shells, which exhibited the highest mobilities, were subjected to a longer growth time and therefore more prolonged annealing. Bare GaAs nanowires, which exhibited the lowest mobilities, were not subjected to any high temperature annealing at all. To investigate the effect of annealing, we performed additional studies for which details can be found in the Supporting Information (Figure S4). These experiments confirmed that high temperature annealing does not account for the improvements in carrier lifetime and mobility. Improvements in carrier mobility and lifetime can be confidently attributed to the high quality AlGaAs shells.

In conclusion, we have measured the photoconductivity of GaAs/AlGaAs core–shell nanowires, which revealed exceptionally high charge carrier mobilities and lifetimes. Increasing the AlGaAs shell thickness significantly improved both the electron mobility and the photoconductivity lifetime. Optimized AlGaAs-clad GaAs nanowires exhibited very long photoconductivity lifetimes of up to 1.6 ns at room temperature, which is almost 3 orders of magnitude longer than the photoconductivity lifetime of bare GaAs nanowires. The measured photoluminescence and photoconductivity dynamics indicate that the AlGaAs shells effectively remove deep surface states, to eliminate surface band-bending and depletion effects. Optimized AlGaAs-coated nanowires exhibited electron mobilities at least 65% of that of high quality bulk GaAs. These results suggest the potential of modulation doping of nanowire shells,[45−47] as an effective means of introducing free carriers to the nanowire core while maintaining very high carrier mobilities in the core. High carrier mobilities and long carrier lifetimes will improve the performance of GaAs nanowire-based electronic and optoelectronic devices, and may potentially enable the study of ballistic transport and other fundamental physical phenomena at cryogenic temperatures.[43]

■ ASSOCIATED CONTENT

Ⓢ Supporting Information

Description of experiments (nanowire growth, terahertz time-domain spectroscopy, photoluminescence spectroscopy), transmission electron microscopy data, photoluminescence spectral data, mobility data comparing core–shell–cap and core–shell nanowires, and photoconductivity spectra and decays for annealed bare GaAs nanowires. This material is available free of charge via the Internet at http://pubs.acs.org.

dx.doi.org/10.1021/nl503043p | Nano Lett. 2014, 14, 5989−5994

AUTHOR INFORMATION

Corresponding Authors

*E-mail: hannah.joyce@eng.cam.ac.uk.

*E-mail: m.johnston@physics.ox.ac.uk.

Notes

The authors declare no competing financial interest.

ACKNOWLEDGMENTS

The authors thank the EPSRC (U.K.) (H.J.J., P.P., C.J.D., L.M.H., M.B.J.) and the Australian Research Council (N.J., Q.G., H.H.T., C.J.) for funding. H.J.J. thanks the Royal Commission for the Exhibition of 1851 for her research fellowship. The Australian National Fabrication Facility, ACT Node, is acknowledged for access to the growth facility used is this work. The Australian Microscopy and Microanalysis Research Facility, ACT Node, is acknowledged for access to the TEM facilities used in this work.

REFERENCES

(1) Chuang, L. C.; Sedgwick, F. G.; Chen, R.; Ko, W. S.; Moewe, M.; Ng, K. W.; Tran, T. D.; Chang-Hasnain, C. *Nano Lett.* **2011**, *11*, 385−390.

(2) Dai, X.; Zhang, S.; Wang, Z.; Adamo, G.; Liu, H.; Huang, Y.; Couteau, C.; Soci, C. *Nano Lett.* **2014**, *14*, 2688−2693.

(3) Gudiksen, M. S.; Lauhon, L. J.; Wang, J.; Smith, D. C.; Lieber, C. M. *Nature* **2002**, *415*, 617−620.

(4) Krogstrup, P.; Jorgensen, H. I.; Heiss, M.; Demichel, O.; Holm, J. V.; Aagesen, M.; Nygard, J.; Morral, A. F. I. *Nat. Photonics* **2013**, *7*, 306−310.

(5) Yao, M.; Huang, N.; Cong, S.; Chi, C.; Seyedi, M. A.; Lin, Y.; Cao, Y.; Povinelli, M. L.; Dapkus, P. D.; Zhou, C. *Nano Lett.* **2014**, *14*, 3293−3303.

(6) Ren, S.; Zhao, N.; Crawford, S. C.; Tambe, M.; Bulović, V.; Gradečak. *Nano Lett.* **2011**, *11*, 408−413.

(7) Heiss, M.; et al. *Nat. Mater.* **2013**, *12*, 439−444.

(8) Saxena, D.; Mokkapati, S.; Parkinson, P.; Jiang, N.; Gao, Q.; Tan, H. H.; Jagadish, C. *Nat. Photonics* **2013**, *7*, 963−968.

(9) Mayer, B.; Rudolph, D.; Schnell, J.; Morkotter, S.; Winnerl, J.; Treu, J.; Muller, K.; Bracher, G.; Abstreiter, G.; Koblmüller, G.; Finley, J. J. *Nat. Commun.* **2013**, *4*, 2931.

(10) Demichel, O.; Heiss, M.; Bleuse, J.; Mariette, H.; Fontcuberta i Morral, A. *Appl. Phys. Lett.* **2010**, *97*, 201907.

(11) Katzenmeyer, A. M.; Léonard, F.; Talin, A. A.; Wong, P.; Huffaker, D. L. *Nano Lett.* **2010**, *10*, 4935−4938.

(12) Gutsche, C.; Niepelt, R.; Gnauck, M.; Lysov, A.; Prost, W.; Ronning, C.; Tegude, F. *Nano Lett.* **2012**, *12*, 1453−1458.

(13) Chang, C.; Chi, C.; Yao, M.; Huang, N.; Chen, C.; Theiss, J.; Bushmaker, A. W.; LaLumondiere, S.; Yeh, T.; Povinelli, M. L.; Zhou, C.; Dapkus, P. D.; Cronin, S. B. *Nano Lett.* **2012**, *12*, 4484−4489.

(14) Han, N.; Wang, F.; Hou, J. J.; Xiu, F.; Yip, S.; Hui, A. T.; Hung, T.; Ho, J. C. *ACS Nano* **2012**, *6*, 4428−4433.

(15) Dayeh, S. A.; Soci, C.; Bao, X. Y.; Wang, D. L. *Nano Today* **2009**, *4*, 347−358.

(16) Joyce, H. J.; Docherty, C. J.; Gao, Q.; Tan, H. H.; Jagadish, C.; Lloyd-Hughes, J.; Herz, L. M.; Johnston, M. B. *Nanotechnology* **2013**, *24*, 214006.

(17) Parkinson, P.; Joyce, H. J.; Gao, Q.; Tan, H. H.; Zhang, X.; Zou, J.; Jagadish, C.; Herz, L. M.; Johnston, M. B. *Nano Lett.* **2009**, *9*, 3349−3353.

(18) Titova, L. V.; Hoang, T. B.; Jackson, H. E.; Smith, L. M.; Yarrison-Rice, J. M.; Kim, Y.; Joyce, H. J.; Tan, H. H.; Jagadish, C. *Appl. Phys. Lett.* **2006**, *89*, 173126.

(19) Tambe, M. J.; Lim, S. K.; Smith, M. J.; Allard, L. F.; Gradečak. *Appl. Phys. Lett.* **2008**, *93*, 151917.

(20) Breuer, S.; Pfüller, C.; Flissikowski, T.; Brandt, O.; Grahn, H. T.; Geelhaar, L.; Riechert, H. *Nano Lett.* **2011**, *11*, 1276−1279.

(21) Bolinsson, J.; Ek, M.; Trägårdh, J.; Mergenthaler, K.; Jacobsson, D.; Pistol, M.; Samuelson, L.; Gustafsson, A. *Nano Res.* **2014**, *7*, 1−18.

(22) Perera, S.; Fickenscher, M. A.; Jackson, H. E.; Smith, L. M.; Yarrison-Rice, J. M.; Joyce, H. J.; Gao, Q.; Tan, H. H.; Jagadish, C.; Zhang, X.; Zou, J. *Appl. Phys. Lett.* **2008**, *93*, 053110.

(23) Jiang, N.; Parkinson, P.; Gao, Q.; Breuer, S.; Tan, H. H.; Wong-Leung, J.; Jagadish, C. *Appl. Phys. Lett.* **2012**, *101*, 023111.

(24) Ketterer, B.; Uccelli, E.; Fontcuberta i Morral, A. *Nanoscale* **2012**, *4*, 1789−1793.

(25) van Tilburg, J. W. W.; Algra, R. E.; Immink, W. G. G.; Verheijen, M.; Bakkers, E. P. A. M.; Kouwenhoven, L. P. *Semicond. Sci. Technol.* **2010**, *25*, 024011.

(26) Storm, K.; Halvardsson, F.; Heurlin, M.; Lindgren, D.; Gustafsson, A.; Wu, P. M.; Monemar, B.; Samuelson, L. *Nat. Nanotechnol.* **2012**, *7*, 718−722.

(27) Joyce, H. J.; Gao, Q.; Tan, H. H.; Jagadish, C.; Kim, Y.; Zou, J.; Smith, L. M.; Jackson, H. E.; Yarrison-Rice, J. M.; Parkinson, P.; Johnston, M. B. *Prog. Quantum Electron.* **2011**, *35*, 23−75.

(28) Joyce, H. J.; Gao, Q.; Tan, H. H.; Jagadish, C.; Kim, Y.; Zhang, X.; Guo, Y. N.; Zou, J. *Nano Lett.* **2007**, *7*, 921−926.

(29) Jiang, N.; Gao, Q.; Parkinson, P.; Wong-Leung, J.; Mokkapati, S.; Breuer, S.; Tan, H. H.; Zheng, C. L.; Etheridge, J.; Jagadish, C. *Nano Lett.* **2013**, *13*, 5135−5140.

(30) Joyce, H. J.; Wong-Leung, J.; Yong, C.; Docherty, C. J.; Paiman, S.; Gao, M.; Tan, H. H.; Jagadish, C.; Lloyd-Hughes, J.; Herz, L. M.; Johnston, M. B. *Nano Lett.* **2012**, *12*, 5325−5330.

(31) Henry, C. H.; Logan, R. A.; Merritt, F. R. *J. Appl. Phys.* **1978**, *49*, 3530−3542.

(32) Ahrenkiel, R. K. *Solid-State Electron.* **1992**, *35*, 239−250.

(33) Yong, C. K.; Wong-Leung, J.; Joyce, H. J.; Lloyd-Hughes, J.; Gao, Q.; Tan, H. H.; Jagadish, C.; Johnston, M. B.; Herz, L. M. *Nano Lett.* **2013**, *13*, 4280−4287.

(34) Pemasiri, K.; Montazeri, M.; Gass, R.; Smith, L. M.; Jackson, H. E.; Yarrison-Rice, J.; Paiman, S.; Gao, Q.; Tan, H. H.; Jagadish, C.; Zhang, X.; Zou, J. *Nano Lett.* **2009**, *9*, 648−654.

(35) Yong, C. K.; Noori, K.; Gao, Q.; Joyce, H. J.; Tan, H. H.; Jagadish, C.; Giustino, F.; Johnston, M. B.; Herz, L. M. *Nano Lett.* **2012**, *12*, 6293−6301.

(36) Yablonovitch, E.; Sandroff, C. J.; Bhat, R.; Gmitter, T. *Appl. Phys. Lett.* **1987**, *51*, 439−441.

(37) Parkinson, P.; Lloyd-Hughes, J.; Gao, Q.; Tan, H. H.; Jagadish, C.; Johnston, M. B.; Herz, L. M. *Nano Lett.* **2007**, *7*, 2162−2165.

(38) Strait, J. H.; George, P. A.; Levendorf, M.; Blood-Forsythe, M.; Rana, F.; Park, J. *Nano Lett.* **2009**, *9*, 2967−2972.

(39) Parkinson, P.; Dodson, C.; Joyce, H. J.; Bertness, K. A.; Sanford, N. A.; Herz, L. M.; Johnston, M. B. *Nano Lett.* **2012**, *12*, 4600−4604.

(40) Nuss, M. C.; Auston, D. H.; Capasso, F. *Phys. Rev. Lett.* **1987**, *58*, 2355−2358.

(41) Sharma, G.; Al-Naib, I.; Hafez, H.; Morandotti, R.; Cooke, D. G.; Ozaki, T. *Opt. Express* **2012**, *20*, 18016−18024.

(42) Caughey, D. M.; Thomas, R. E. *Proc. IEEE* **1967**, *55*, 2192−2193.

(43) Shtrikman, H.; Popovitz-Biro, R.; Kretinin, A. V.; Kacman, P. *IEEE J. Sel. Top. Quantum Electron.* **2011**, *17*, 922−934.

(44) Xiang, J.; Lu, W.; Hu, Y. J.; Wu, Y.; Yan, H.; Lieber, C. M. *Nature* **2006**, *441*, 489−493.

(45) Jadczak, J.; Plochocka, P.; Mitioglu, A.; Breslavetz, I.; Royo, M.; Bertoni, A.; Goldoni, G.; Smolenski, T.; Kossacki, P.; Kretinin, A.; Shtrikman, H.; Maude, D. K. *Nano Lett.* **2014**, *14*, 2807−2814.

(46) Sladek, K.; Klinger, V.; Wensorra, J.; Akabori, M.; Hardtdegen, H.; Grutzmacher, D. *J. Cryst. Growth* **2010**, *312*, 635−640.

(47) Spirkoska, D.; Fontcuberta i Morral, A.; Dufouleur, J.; Xie, Q.; Abstreiter, G. *Phys. Status Solidi RRL* **2011**, *5*, 353−355.